

Article

Improved Adsorption of the Antimicrobial Agent Poly (Hexamethylene) Biguanide on Ti-Al-V Alloys by NaOH Treatment and Impact of Mass Coverage and Contamination on Cytocompatibility

Paula Zwicker ^{1,*}, Norman Geist ^{2,†}, Elisabeth Göbler ², Martin Kulke ^{2,‡}, Thomas Schmidt ¹, Melanie Hornschuh ¹, Ulrich Lembke ³, Cornelia Prinz ³, Mihaela Delcea ², Axel Kramer ¹ and Gerald Müller ¹

¹ Institute of Hygiene and Environmental Medicine, University Medicine, 17489 Greifswald, Germany; thomas.schmidt@med.uni-greifswald.de (T.S.); Melanie.hornschuh@med.uni-rostock.de (M.H.); axel.kramer@med.uni-greifswald.de (A.K.); muellerg@hotmail.com (G.M.)

² Biophysical Chemistry Department, Institute of Biochemistry, University of Greifswald, 17489 Greifswald, Germany; Norman.geist@uni-greifswald.de (N.G.); eli.goebler@hotmail.de (E.G.); kulkemar@msu.edu (M.K.); mihaela.delcea@uni-greifswald.de (M.D.)

³ DOT GmbH Medical Implant Solutions, 18059 Rostock, Germany; lembke@dot-coating.de (U.L.); prinz@dot-coating.de (C.P.)

* Correspondence: paula.zwicker@med.uni-greifswald.de

† These authors contributed equally to this work.

‡ Current address: MSU-DOE Plant Research Laboratory, Michigan State University, 612 Wilson Rd, East Lansing, MI 48824, USA.



Citation: Zwicker, P.; Geist, N.; Göbler, E.; Kulke, M.; Schmidt, T.; Hornschuh, M.; Lembke, U.; Prinz, C.; Delcea, M.; Kramer, A.; et al. Improved Adsorption of the Antimicrobial Agent Poly (Hexamethylene) Biguanide on Ti-Al-V Alloys by NaOH Treatment and Impact of Mass Coverage and Contamination on Cytocompatibility. *Coatings* **2021**, *11*, 1118. <https://doi.org/10.3390/coatings11091118>

Academic Editor: Alina Vladescu

Received: 10 August 2021

Accepted: 10 September 2021

Published: 15 September 2021

Publisher's Note: MDPI stays neutral with regard to jurisdictional claims in published maps and institutional affiliations.



Copyright: © 2021 by the authors. Licensee MDPI, Basel, Switzerland. This article is an open access article distributed under the terms and conditions of the Creative Commons Attribution (CC BY) license (<https://creativecommons.org/licenses/by/4.0/>).

Abstract: Unlike the native surface of the implant material (Ti6Al4V), oxidation with H₂O₂ leads to increased binding of the effective antimicrobial agent poly(hexamethylene) biguanide [PHMB]. However, treating with NaOH instead results in an even higher PHMB mass coverage. After oxidation with H₂O₂, strong differences in the PHMB adsorption capability between polished and corundum-blasted surfaces appear, indicating a roughness dependence. After NaOH treatment, no such effect was observed. The wetting properties of specimens treated with either H₂O₂ or NaOH prior to PHMB exposure clearly varied. To unravel the nature of this interaction, widespread in silico and in vitro experiments were performed. **Methods:** By X-ray photoelectron spectroscopy, scanning electron microscopy, water contact angle measurements and MD simulations, we characterized the interplay between the polycationic antimicrobial agent and the implant surface. A theoretical model for PHMB micelles is tested for its wetting properties and compared to carbon contaminated TiO₂. In addition, quantitation of anionic functional group equivalents, the binding properties of PHMB with blocked amino end-group, and the ability to bind chlorhexidine digluconate (CHG) were investigated. Ultimately, the capability of osteoblasts to build calcium apatite, and the activity of alkaline phosphatase on PHMB coated specimens, were determined. **Results:** Simulated water contact angles on carbon contaminated TiO₂ surfaces and PHMB micelle models reveal little influence of PHMB on the wetting properties and point out the major influence of remaining and recovering contamination from ambient air. Testing PHMB adsorption beyond the critical micelle concentration and subsequent staining reveals an island-like pattern with H₂O₂ as compared to an evenly modified surface with NaOH. Both CHG and PHMB, with blocked amino end groups, were adsorbed on the treated surfaces, thus negating the significant influence of PHMB's terminal groups. The ability of osteoblasts to produce calcium apatite and alkaline phosphatase is not negatively impaired for PHMB mass coverages up to 8 µg/specimen. **Conclusion:** Differences in PHMB adsorption are triggered by the number of anionic groups and carbon contaminants, both of which depend on the specimen pre-treatment. With more PHMB covering, the implant surface is protected against the capture of new contamination from the ambient air, thus building a robust antimicrobial and biocompatible surface coating.

Keywords: Poly(hexamethylene)biguanide; PHMB; Molecular dynamics simulation; osseointegration; antimicrobial coating; wetting; Ti6Al4V; TiO₂; Rose Bengal staining; water contact angle; carbon contamination; implant coating; micelle

1. Introduction

While titanium implants become more and more popular in surgical care, implant-associated infections are rising. Titanium and titanium-based materials like Ti6Al4V alloys readily build oxidation layers upon air exposure, which are dominated by the TiO₂ form of the crystal [1,2]. Therefore, TiO₂ is the relevant interface of implants based on Ti6Al4V alloys that need to be investigated. In addition, nearly every XPS measurement on TiO₂ reveals a significant carbon content associated with the contamination by volatile hydrocarbons from ambient air [3,4]. Depending on the degree of contamination, a large variance in the characterization of hydrophobic surface properties is found in the literature. While water contact angles on freshly cleaned TiO₂ are usually reported in the range of 15°–30° or below, air-exposed and untreated samples can give readings in the range of 40°–60° and higher [5,6]. Both, inorganic and organic contamination can lead to implant failure by reducing cell attachment leading to impaired osseointegration [7]. It is therefore of interest to prepare the surface of a Ti6Al4V implant, so that the interface properties remain persistent, as they were tested and the surface is protected from being subsequently altered. Moreover, inducing antimicrobial properties to implant materials helps to reduce infection and rejection complications of implanted prostheses. As a result, many techniques were investigated to coat and pre-treat implant materials with, e.g., antimicrobial agents. Besides the desired antimicrobial effects, the surface conservation, an improved adhesion and activity of osteoblastic cells, as well as a compatibility towards immune cells for enhanced osseointegration, would be of additional advantage for a desirable implant coating [8–10].

A potent antiseptic to use as an antimicrobial coating, is poly(hexamethylene) biguanide (PHMB). It was already examined earlier as a coating for Ti6Al4V alloy material [8]. PHMB is a polycationic polymeric molecule with alternating hydrophilic and hydrophobic segments enabling adsorption onto negatively charged surfaces [11].

In previous studies by Müller et al. and Hornschuh et al., the surface of Ti6Al4V alloy material was modified by oxidation with H₂O₂ and pre-treatment with NaOH, respectively, following adsorption of PHMB to the surface by incubation in aqueous solution [8,9,12]. Müller et al. stated that a hydroxylated surface is necessary for PHMB adsorption, as a simple cleaning of the surface without the generation of extra binding sites did not result in stronger PHMB binding [8]. Thus, in contrast to unmodified surfaces, oxidation with H₂O₂ resulted in a 10 times higher PHMB coverage of 1.36 ± 0.12 µg per test specimen [8]. Hornschuh et al. demonstrated a binding capacity of H₂O₂ oxidized surfaces up to 3–4 µg per test specimen [12]. The increased adsorption was ascribed to a removal of impurities on the titanium surface and to the generation of more possible binding sites in the form of OH[−]-groups, as revealed by Tengvall et al. [13]. Naturally, a hydroxylation equilibrium beyond pH 6 also comes along with an increasing negative net charge of the titanium oxide following attraction of the positively charged PHMB polymer [14]. An even higher binding capacity was reached by incubation of the specimens in NaOH, rather than H₂O₂. With this method, the amount of PHMB adsorption is adjustable by incubation time in the coating solution. After 24 h, a PHMB adsorption of up to 20.9 ± 0.6 µg per test specimen was detected, and after 48 h, equilibrium was reached [9,12]. While the increased hydroxylation enhances PHMB adsorption, it also attracts more volatile hydrocarbons, leading to a fast contamination of the surface. Next to these binding experiments, the antimicrobial activity of the PHMB coating could also be demonstrated [8,9,12] using different microbial species. Besides the antimicrobial efficacy, the viability of adsorbed osteoblast cells (MG-63, SaOs-2) on PHMB-coated Ti6Al4V alloy was also confirmed [8,9].

To date, it is not clear, why the pre-treatment of Ti6Al4V-specimens with H₂O₂ or NaOH results in a large difference of PHMB mass coverage at the surface, and how PHMB binding influences the wetting properties in terms of water contact angles (WCA). In this study, we investigated the wetting properties of pure PHMB interfaces, and of contaminated models, for the Ti6Al4V-specimen by means of simulated contact angles. Artificial PHMB surfaces representing cutouts of larger micelles or amorphous films were developed, to understand how likely the mode of binding is to explain the differences the wetting properties. The binding mode might depend on the specific end-groups of PHMB and their affinity to attach to the specimen's surface. In comparison, simulations of water contact angles on carbon contaminated TiO₂ surfaces are performed. The influence of hydrocarbon contamination on the wetting properties of this model were also investigated previously [15], and the WCAs were measured by hand fitting circles onto 2D image snapshots at the end of short simulations. We introduce here an automated measurement from simulation data by a 3D ellipsoid fit, to access the over-time relaxation process of the water droplet. This allows a more precise and reliable estimation of the equilibrium water contact angle.

Further, various *in vitro* analyses were performed for the characterization of the PHMB adsorption on the Ti6Al4V surfaces. To gain better understanding of the binding modes, the quantities of equivalent anionic groups after H₂O₂ or NaOH treatment were determined and the binding capacity of the surface to PHMB was compared to that of the structurally similar chlorhexidine digluconate (CHG). A possible binding via the amino end-group was suppressed by the use of fluorescein isothiocyanate (FITC)-PHMB. In contrast to previous studies which examine polished surfaces, corundum-blasted Ti6Al4V test specimens were examined, as well as incubations in higher PHMB concentrations (6%). The binding of higher PHMB amounts revealed differences in cell viability. Together with XPS and WCA data, a comprehensive model for the observed effects on PHMB coating was established.

2. Materials and Methods

2.1. *In vitro* Experiments

2.1.1. Ti6Al4V Test Specimens

Ti6Al4V discs of 11 mm in diameter and 2 mm thickness were purchased from DOT GmbH (Rostock, Germany). Test specimens were ultrasonically cleaned for 30 min in 2% Hellmanex III solution (Hellma, Müllheim, Germany). Afterward, they were rinsed in acetone and sterile water (B.Braun, Melsungen, Germany). The surface roughness of the specimens was measured with a Dektak 3ST surface profiler (Veeco, Plainview, NY, USA) using a velocity of 0.08 mm/s and a stylus force of 30 mg. The resulting parameters for polished (p) surfaces were: arithmetical mean roughness (Ra) = 0.43 ± 0.20 µm, average maximum high of roughness profile (Rz) = 0.42 ± 0.4 µm, and total high of roughness profile (Rt) = 2.41 ± 0.34 µm; and for corundum-blasted (cb) surfaces: Ra = 2.08 ± 0.20 µm, Rz = 14.99 ± 2.57 µm, and Rt = 20.01 ± 7.22 µm.

2.1.2. Poly (Hexamethylene) Biguanide Hydrochloride and Chlorhexidine Digluconate

Six different PHMB oligomers have been identified due to different combinations of amine, cyanoamine, guanidine and cyanoguanidine end-groups [16]. A representative PHMB oligomer consists of nine hexamethylene biguanide units terminated with amino and cyanoguanidine end-groupings [17]. For coating of test specimen, a Polyhexanid solution (Fagron, Germany, Lot 15C20-B06-309679) containing 20% (w/v) PHMB (Arch Biocides Ltd., UK, Lot 14GR274618) in water was used. This stock solution was diluted to 6% or 30 µg/mL for further use. The cationic antiseptic chlorhexidine digluconate (CHG, C9394, Sigma Aldrich, Taufkirchen, Germany) consists of one hexamethylene biguanide unit terminated with p-chlorophenyl rests. For coating experiments, the 20% (w/v) CHG stock solution was diluted to 50 µg/mL.

2.1.3. Surface Treatment Procedures

For the oxidation procedure of p- and cb-Ti6Al4V discs [8], specimens were treated with 1.0 mL aqueous 5% (v/v) hydrogen peroxide solution (Sigma Aldrich, Taufkirchen, Germany) for 24 h at room temperature (21 °C) protected from light in a 24-well cell culture plate following rinsing with sterile water (1.5 mL) four times on an orbital shaker for 5 min, each. Alkaline treatment [9] was carried out in 2.0 mL pre-warmed 5 M NaOH at 60 °C for 2 h (p surface) and 1 h (cb surface), respectively. Test specimens were again washed four times in sterile water on an orbital shaker for 5 min.

2.1.4. Quantification of Adsorbed Biguanides

The amount of adsorbed PHMB or CHG was calculated by using the difference in absorption of applied and residual concentration of the antiseptic agent. Absorbance of 250 µL aliquots were measured in a 96-well quartz microplate (Hellma, Müllheim, Germany) at 235 nm for PHMB and 233 nm for CHG with a microplate reader (PowerWave XS, BioTek Instruments Inc., Winooski, VT, USA).

2.1.5. Surface Analysis

For determination of the elemental composition of the specimens' surface, X-ray photoelectron spectroscopy (XPS) analysis was used as described previously [9]. The specimens were stored in 20 ml-scintillation vials in sterile water flushed with nitrogen. To remove aliphatic carbon contaminations, the scintillation vials were ultrasonically cleaned for 30 min with 2% Hellmanex III solution (Hellma, Müllheim, Germany) and afterwards rinsed with acetone two times and sterile water 4 times, each for 30 s. The Axis Ultra (Kratos Analytical Ltd., Manchester, UK) ran with the monochromatic Al-K line at 1486 eV (150 W) under high vacuum conditions. The peak fitting procedure was carried out with CasaXPS software version 2.2 (Casa Software Ltd., UK) using the Gauss–Lorentz (30% Lorentz) distribution, Shirley baseline and a fixed FWHM (full width at half maximum). All values are presented in at.-% and corresponding element ratios.

2.1.6. Determination of Anionic Functional Groups on the Ti6Al4V Surface

The photometrical analysis of anionic groups on solid surfaces was adopted from Sano et al. [18]. Anionic groups on the Ti6Al4V surface were complexed with 0.5 mM Toluene Blue O (TBO, Sigma, Taufkirchen, Germany), pH 10, at room temperature, protected from light on an orbital shaker for 5 h, followed by rinsing with 1 mM NaOH to remove non-complexed TBO. Desorption of dye molecules complexed to anionic surface groups was conducted with 2.0 mL of 1% (w/v) sodium dodecyl sulfate (SDS, Sigma Aldrich, Taufkirchen, Germany) aqueous solution for 16–20 h on an orbital shaker. The molar absorption coefficient of TBO in 1% SDS of $52.23 \text{ M}^{-1} \text{ cm}^{-1}$ was used for its quantitation at 630 nm.

2.1.7. Detection of Adsorbed Biguanides on the Ti6Al4V Surface Using Rose Bengal

Concentrations of biguanides in solution were assessed colorimetrically, adapted from Gilbert et al., using the xanthene derivative Rose Bengal instead of Eosin Y [19,20]. The staining of adsorbed biguanides on each Ti6Al4V specimen was conducted in 2.5 mL of Rose Bengal reagent (0.017 mM Rose Bengal in 30 mM Na-acetate, pH 8.6) in 24-well cell culture plates (Sarstedt, Nümbrecht, Germany). After 24 h incubation, the specimens were removed and the residual dye concentration was determined spectrophotometrically at 549 nm. Potentially released combinations of each biguanide with Rose Bengal were measured at 576 nm. For calculation of the amount of dye consumption, a calibration curve at 549 nm was used. The biguanide binding calibration curve for evaluation of biguanide-dye-complexes was assessed at 576 nm.

2.1.8. SEM for Assessment of the Surface Structure

The surface morphologies of differently prepared Ti6Al4V specimens were analyzed by scanning electron microscopy (SEM). The samples were stored in the same way as described for the XPS analysis in order to diminish surface contamination. Before transferring the samples into the vacuum chamber of the Tesla VEGA 3 microscope (TESCAN, Brunn, Czech Republic), the specimens were dried dust-free. Using an acceleration energy of 10 keV, the SEM micrographs were taken with appropriate magnification by a secondary electron (SE) detector.

2.1.9. Wettability

Wettability of the surface of Ti6Al4V specimens was examined by an optical water contact angle (WCA) measuring device (Dataphysics OCA40 Micro, Germany) using 1 μ L of deionized water at 25 °C and 45% humidity. WCAs were measured with the profiles of droplets deposited on the control and modified surfaces immediately after stabilization by SCA software (Dataphysics, Germany). For statistical analysis of differences in water contact angles, a one-way ANOVA following Dunnett's multiple comparison were used post-hoc.

2.1.10. Binding of FITC to PHMB and Coating of the Test Specimen

The terminal amino group of PHMB was blocked with fluorescein isothiocyanate (FITC, Sigma Aldrich, Taufkirchen, Germany) adapted from Chindera et al. [21]. FITC (2 mg) was dissolved in 750 μ L N,N-dimethylformamide and 50 μ L N,N-diisopropylethylamine. PHMB (50 mg in 200 μ L sterile water) was added to the mixture and the solution was shaken overnight at room temperature, protected from light. Separation of unbound FITC and FITC-labelled PHMB was conducted gelchromatographically with a Sephadex™ G-25 column (GE Healthcare, IL, USA), as instructed by the manufacturer. In short, the gel bed was equilibrated with 25 mL PBS, then an aliquot of 1.0 mL FITC-PHMB reaction mixture and another 1.5 mL PBS were added. FITC-PHMB was eluted with 3.5 mL PBS. The flow through was sampled in three fractions. Fraction 2 was diluted to 30 μ g/mL PHMB-equivalents as determined with Rose Bengal staining spectrophotometrically and used for coating experiments. To monitor adsorbed FITC-PHMB, the test specimens were analyzed using a fluorescence microscope (Hund, Wetzlar) at 400 \times magnification.

2.1.11. SaOs-2 Cell Culture, Cell Viability, Alkaline Phosphatase Activity and Mineralization Assay

Cell culture was conducted at 37 °C in a humidified atmosphere with 5% CO₂. Human osteoblast-like cells (SaOs-2, CLS Cell Line Service, Eppenheim, Germany) were cultured in DMEM/F12 with 2 mM L-glutamine and 5% fetal bovine serum. After trypsinization, the cell suspension was adjusted to 2 \times 10⁶ cells/ml in cell culture medium; 50 μ L of this suspension was added to polished control Ti6Al4V test specimens as well as to polished NaOH pre-treated and PHMB-coated specimens, that were coated in PHMB solution for 2 h and 20 h, respectively. After cell culturing for 60 min, 1.0 mL fresh medium was added and cell culturing was continued for 3 days in 24-well cell culture plates. Afterward, the cell culture medium was supplemented with 50 μ g/mL ascorbic acid, 10 mM Na-beta-D-glycerophosphate, and 20 mM dexamethasone and renewed every day for the next four days. Cell viability was analyzed using the 2,3-Bis-(2-methoxy-4-nitro-5-sulfophenyl)-2H-tetrazolium-5-carboxanilid (XTT, Sigma Aldrich, Taufkirchen, Germany) assay in 1.5 mL of a XTT solution (0.33 mg/mL, 1.27 μ g phenazine methosulfate) at 37 °C for 3 h. Absorption of the produced colored formazan was measured at 450 nm. For detection of alkaline phosphatase (ALP) activity, cells on test specimens were washed twice with PBS (with Ca²⁺ and Mg²⁺, wPBS) and then incubated for fixation in 1.0 mL ice-cold ethanol (70%, v/v) for 1 h at 4 °C. The specimens were dried, and ALP was stained for 30 min at 37 °C with 0.1 M Tris-buffer (pH 8.4), containing 0.9 mM naphthol AS-MX phosphate (Sigma Aldrich,

Taufkirchen, Germany), 1.8 mM Fast Red TR salt (Sigma Aldrich, Taufkirchen, Germany), 25 mM NaCl, and 4 mM MgCl₂, thereby staining active regions red. Quantitative analysis was conducted by incubating the fixed cells for 15 min with 0.5 mL substrate solution (SigmaFast™ p-nitrophenyl phosphate tablet, Sigma Aldrich, Taufkirchen, Germany) at 37 °C. The enzymatic reaction was stopped by adding 125 µL of a 3 M NaOH solution, and absorption was measured at 405 nm in aliquots of 250 µL in a 96-well microtiter plate. The ALP activity was calculated by use of a calibration curve, that was set up with p-nitrophenyl phosphate (PNP) in 0.1 M NaOH. Mineralization of the cells (calcium apatite, CaP) was analyzed by staining with Alizarin Red S (Sigma Aldrich, Taufkirchen, Germany). A 40 mM solution (pH 4.1–4.3) was added to the cells following incubation for 30 min. Afterwards, cells were washed, and the dye was eluted by adding 10% (w/v) cetylpyridiniumchloride in a 10 mM phosphate buffer (pH 7.0) while shaking for 1 h. Absorption was measured at 562 nm. ALP and CaP data were normalized for cell viability. The tests were conducted with six technical replicates and two biological replicates each.

2.2. Molecular Dynamics Simulations

2.2.1. PHMB Models and Force Field

The PHMB force field built in this study includes building blocks for the major amino (PHT) and cyanoguanidine (PHA) end-groups as well as a biguanidine-hexamethylene middle repeat unit (PHM). Thereby, the lengths of oligomers are freely selectable. The initial atomic structure was built using Molden 5.4 [22]. Subsequently, the structure of the smallest possible repeat unit was first optimized with the generic Amber/GAFF force field inside Molden followed by a Geometry optimization using Gaussian 2003 [23] with the B3LYP/6-31G* basis set. The resulting structure was subjected to a single-point-optimization with Gaussian, and the HF/6-31G* basis set with the respective output flags in place for the subsequent RESP fit procedure [24]. The fit for the point-charges was carried out using the well known Antechamber program from the Ambergtools 2018 package [25]. Charge restraints were put in place to ensure integer charges on the individual subunits PHA, PHM and PHT and they were accordingly split into separate library units for use with the Amber tool chain. Force field parameters were applied by the GAFF2 procedure [26,27]. Insignificant remaining non-integer charge contributions were subtracted from the average of all positive charges for each subunit. Zeroing the charges was especially critical, as the simulations in this study contained large numbers of oligomers. MDS usually require a zero net charge if periodic boundary conditions are applied and even small remaining inaccuracies in the obtained point charges would have accumulated over the large simulation cells. This would also perturb the stoichiometry of biguanidino groups and chloride ions when neutralizing the system. The parameterisation for pentanol followed the same procedure. The force field files are provided as Supporting Information.

2.2.2. Simulation Settings

Molecular dynamics simulations were carried out using NAMD version 2.13 with CUDA acceleration [28,29]. The short-range cutoffs were set to 1 nm for van der Waals (VDW) and Coulomb interactions, including a smooth switch-off function with a 0.1 nm area towards the cutoff. Long-range electrostatics were considered by smooth particle-mesh-Ewald (sPME) [30] and a 0.1 nm grid spacing under full periodic boundary conditions. The hydrogen mass repartitioning scheme [31] was applied by the ParmEd 2.4.0 program [25], excluding water, and all bonds lengths to hydrogen atoms were constrained by the Rattle algorithm [32]. Due to the suppression of fast hydrogen dynamics, the time step for MD was extended to 4 fs. The temperatures and pressures were controlled by Langevin thermostat [33] with a damping time constant of 1 ps⁻¹ and Langevin piston barostats [34], where period and decay time constants were 100 fs and 200 fs, respectively. Water was represented by the TIP3P water model [35] and total system charges were neutralized by adding appropriate amounts of sodium or chloride ions. Visualization, system

preparation and analysis of pentanol coating and radius of gyration were done with the help of Leap [25] and VMD 1.9.3 [36].

2.2.3. Model Building and Simulated Systems

We started from a medium sized PHMB nonamer [37] that was relaxed by MDS in explicit water solvent from an initially linear conformation. The brush-like model was constructed from an extended conformation that was picked by a typical high R_{gyr} state (Figure 1). By repeating in the spatial XY-dimensions, a building block for our brush-like micelle model was made from 9×9 oligomers and neutralized by appropriate amounts of chloride ions. The system was subjected to relaxation MDS under anisotropic constant pressure conditions and full periodic boundary conditions. This allowed each spatial dimension to optimize independently. Hence, this polymer construct appeared like the part of a much larger micelle structure and would result in a seamless repeatable building block in all spatial dimensions (Figure 2). From this building block, the final PHMB micelle model surfaces for the WCA simulations were constructed as follows.

- The amino and cyanoguanidino end-groups as opposing interfaces by assembling repeats of $6X \times 7Y \times 1Z$ periodic copies resulting in a surface of $33.5 \text{ nm} \times 29.6 \text{ nm} \times 11 \text{ nm}$, representing specific adsorption of end-groups to the Ti6Al4V disc and exposing the respective other end to the water droplet.
- The main chain unit as interface by repeats of $6X \times 2Y \times 3Z$ of size $33.5 \text{ nm} \times 8.4 \text{ nm} \times 33.1 \text{ nm}$, representing flat multi-layered aggregation. This model is also considered representative for an amorphous aggregation, since there is no preference on parts of the polymer to be water exposed.

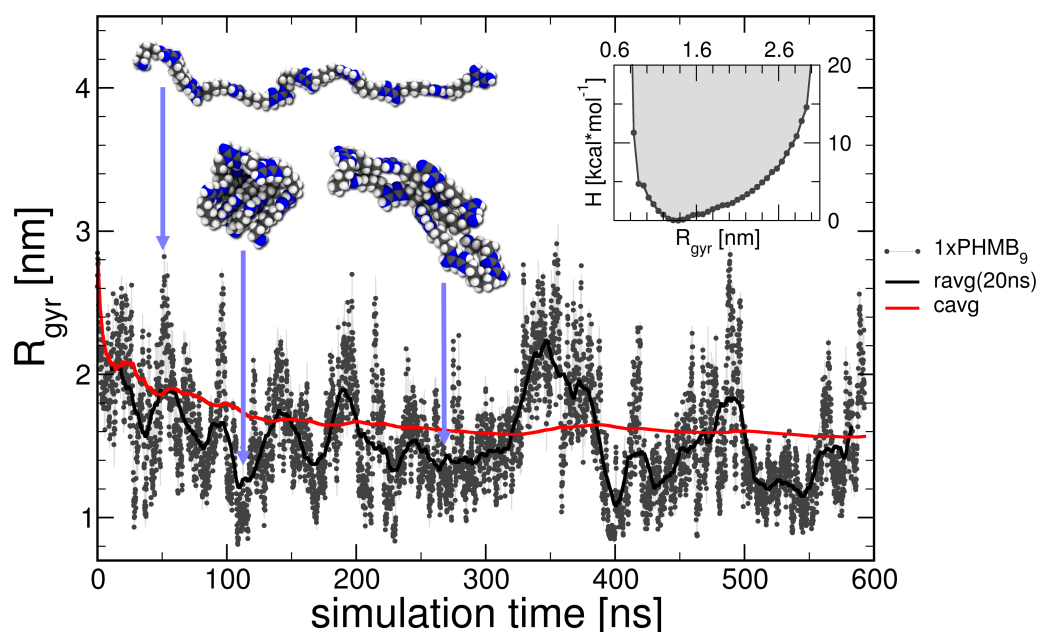


Figure 1. Self-aggregation dynamics of a single PHMB nonamer in aqueous solution by means of R_{gyr} . Snapshots in atomistic representation illustrate high and low R_{gyr} states (N: blue; C: grey; H: white). Point representation of the raw data is plotted only every 100 ps. A running average (rav) with a windows length of 20 ns is applied to smooth the raw data. A cumulative average (cavg) is utilized to appreciate convergence of the ensemble. While the polymer continuously traverses between compact and extended folds, the cavg measure should approach a constant value with increased simulation time. The insert (upper right) shows the free enthalpy obtained by the Boltzman inversion of the R_{gyr} probabilities (50 bins). As seen, only a broad minimum with no significant energy barriers exists to distinguish the different folding states, thus indicating no distinct fold in solution.

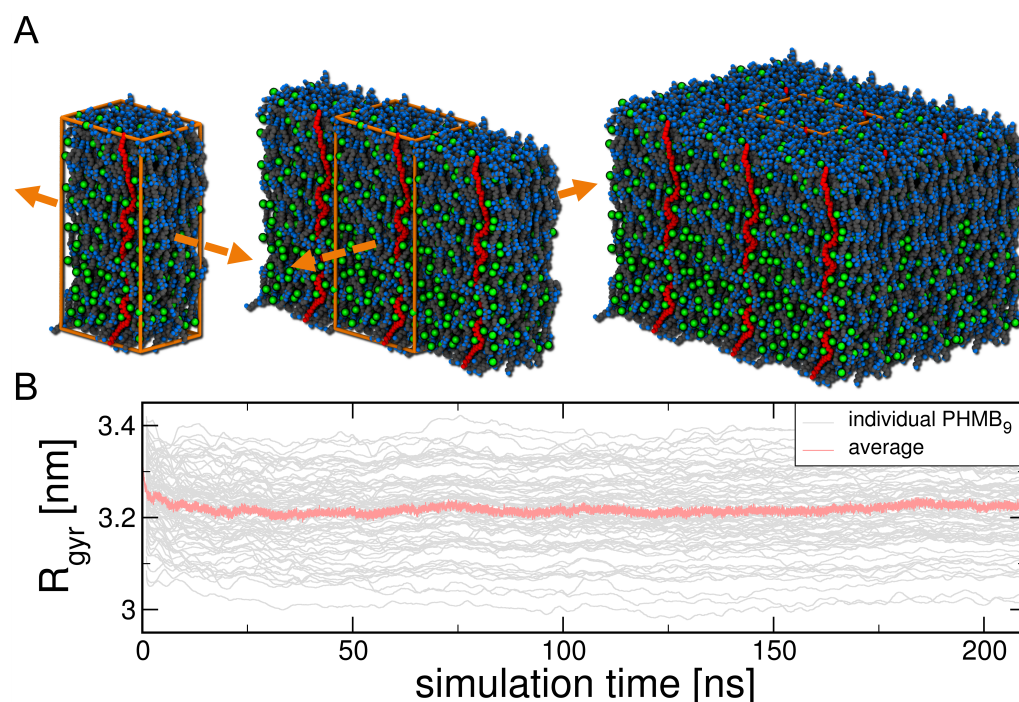


Figure 2. (A) (left) Periodic brush-like structure after 200 ns of relaxation MDS (N: blue; C: grey; H: hidden for clarity; Cl⁻: green). One PHMB₉ oligomer is colored in red to visualize the parallel and extended arrangement. The orange arrows illustrate replication of this building block by the spatial X (left) and Y (middle) dimensions. The resulting surfaces (right), with different end-groups are subjected to the simulation of water contact angles. (B) R_{gyr} of each individual PHMB₉ in our brush-like block is plotted over time with a running average of 2 ns window length. It can be seen that the radii of gyration for all individual oligomers converge quickly and that the structure remains stable. The average R_{gyr} of about 3.2 nm is significantly larger than that for isolated molecules in solution.

Rutile (100) TiO₂ slabs were built using a flexible non-bonded model according to [15], of roughly 32 nm × 32 nm. This model has been used previously by Müller et al. and the Ti6Al4V-specimens used in vitro were sufficiently described by a molecular model of hydroxylated rutile (100) TiO₂ [8]. The hydroxylation equilibrium was adjusted to represent pH 7.4 and this included 1211 and 2280 H⁺ and OH⁻ groups at each side of the surface, respectively. The central titanium layer (five total layers) was kept fixed during the simulations to prevent deformation of this rather thin TiO₂ crystal. The total net charge of the titanium oxide surface of $-892e$ was neutralized by adding 892 Na⁺ ions to the system.

To coat the TiO₂ surface and obtain a reading for the 100% mass coverage for our contamination model, we solvated the titanium oxide slab by repetition of a pre-equilibrated cubic pentanol cell of 2.758 nm side length, containing 117 pentanol molecules at a mass density of 0.816 g/cm³. This pentanol cube was obtained by isotropic NPT equilibration for a few nano seconds from a formerly ordered arrangement of pentanol molecules. The resulting system was subjected to an NPT simulation with fixed XY cell dimensions and allowed volume optimization only in the Z direction. To access the convergence of the coating process, we monitored the number of physically adsorbed pentanol molecules by counting the respective atoms of the alcohol in 0.25 nm proximity to the TiO₂ residues. This represents pentanol molecules coordinating with the titanium oxide by their hydroxy group. Coating simulations of TiO₂ surfaces in pentanol solution proceeded for 32 ns and converged to a maximum coverage of 3.96 pentanol molecules per nm² surface area. Titanium dioxide surface models with reduced amounts of contamination are built from this full coverage by randomly removing pentanol molecules. Thereby, seven systems with pentanol coverage in the range of 0.99–3.96 molecules per nm² were obtained and subjected to simulations of water contact angles.

Simulation of wetting properties in this study were based on the procedure of Friedrichs et al. [15]. Pure PHMB or differently contaminated TiO₂ surface models were placed in simulation cells that matched their spatial XY dimensions to achieve periodic continuation. A water cube with a side length of 7 nm is placed slightly above the center of the surface. Enough water must be added, to allow a reasonable shaped and sized droplet for stable contact angle measurement. The Z dimension of the simulation cell is set to 20 nm for TiO₂ and 60 nm for PHMB surfaces. The large cell size in the Z direction aims to prevent interactions of the water molecules with the periodic images of the surfaces. The sizes of the slabs in the XY direction were chosen to be large enough to hold droplets of even low contact angles without periodic interaction of the water, which otherwise, causes the drop to simply collapse into several water layers.

2.2.4. Time Dependent Contact Angle Analysis

In contrast to previous work, the simulated contact angles in this study were evaluated in an automated fashion over time. Thereby, the relaxation process of the water droplet could be observed, and a reliable measurement for the equilibrium reading of the WCA was obtained. After completion of a simulation, an in-house code was fed with the systems topology. The code splits the molecular system into separate objects for the underlying surface (in the following referred to as slab) and the water droplet. The trajectory is processed frame by frame and the contact angle is obtained for each point in time according to the following procedure: (a) Load updated atomic coordinates from trajectory. (b) Translate the whole system to align the center of the droplet to the center of the simulation cell and wrap the coordinates by periodic boundaries. This shall prevent breaking the droplet and its interface with the slab across the periodic boundaries of the simulation box.

(c) The droplet and slab are scanned for surface points by a 3D rod-decomposition, individually for each spatial dimension (Figure 3). While the rods extend within the whole data bounds in one spatial dimension at a time, the respective other two dimensions of the rods were set to 0.5 nm, controlling the sensitivity of the scanning. The atoms with minimal and maximal coordinates of each rod, in each dimension, deal as the samples to describe the outside of both objects in 3D space. For the slab, only the top view samples (+Z direction) are used, and for the droplet, all directions but the bottom view (-Z direction) are used. During this procedure, outliers were detected based on their distance to the objects center and the standard deviation of this center point, in each spatial dimension separately. Thus, atoms of droplet or slab more distant than three times the standard deviation from the objects center, in a particular spatial dimension, are ignored. This helps to exclude diffusive waters or coating materials of the slab, such as occasionally detaching pentanol molecules. Furthermore, the slab surface is only sampled within the XY bounds of the droplet, this ensures that in case of curvature or roughness of the slab, the contact angle is evaluated relative to the surface area perpendicular to the droplet.

$$0 = ax + by + cz + d$$

$$z = \frac{-ax - by - d}{c} \quad (1)$$

$$z_{surf} = d/c \quad (2)$$

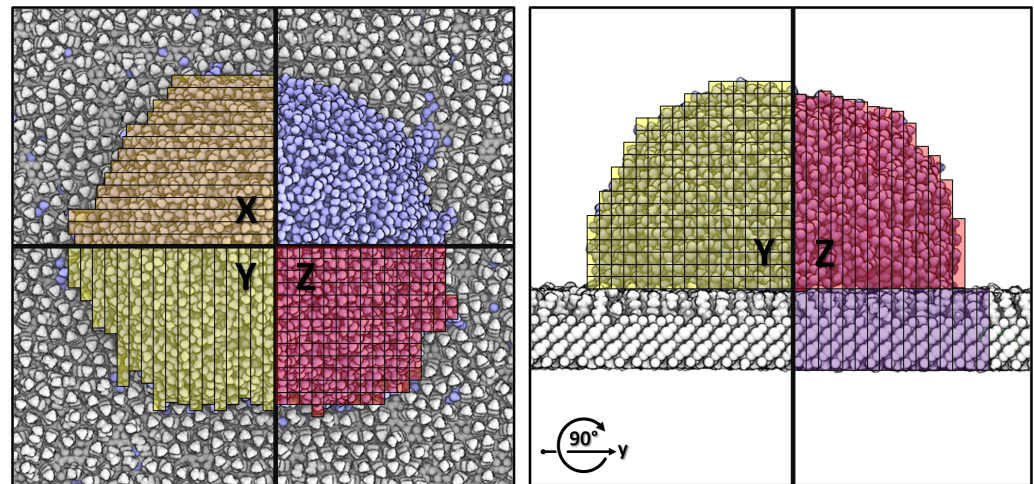


Figure 3. Illustration of the 3D rod decomposition used to sample the outside of the droplet and underlying surface slab for the time dependent analysis of water contact angle simulations. **(left)** Top view of the water droplet (blue atoms) sitting on the surface slab (gray atoms). Although not important for the illustration, the picture shows a fully pentanol covered TiO_2 surface. The colored boxes represent the decomposition of the atoms into rods that span one spatial dimension at a time. All atoms having the minimum or maximum coordinate of a rod, in the respective dimension, are registered as a point on the outside shell of the molecular objects in 3D space. The top right quarter of the droplet is left without rods for better clarity. **(right)** Rotated view along the Y-axis. As illustrated, the surface slab is decomposed following the same scheme. The left side of the surface is left without rods for clarity, but the full surface area below the drop is actually sampled.

(d) Next, the sampled surface points of the slab are subjected to a plane fit (1). Data fitting is performed by interfacing GnuPlot 5.4 [38]. The overall rotation of the resulting plane is removed from the system and the position of the slab surface in the Z-direction Z_{surf} (2) is obtained. (e) The droplet samples are cropped by points below Z_{surf} and a 3D ellipsoid (3) is used to fit the sampled outer shell of the droplet, where x_0 , y_0 and z_0 denote the center of the ellipsoid and a and b represent the radii in the X, Y and Z directions, respectively. This means that the droplet is assumed circular in the X-Y direction and adapted independently in the Z direction.

$$1 = \frac{(x-x_0)^2}{a^2} + \frac{(y-y_0)^2}{a^2} + \frac{(z-z_0)^2}{b^2}$$

$$z = \sqrt{\left(1 - \frac{(x-x_0)^2 + (y-y_0)^2}{a^2}\right) b^2} + z_0 \quad (3)$$

$$x_{surf} = a \sqrt{1 - \frac{(z_{surf}-z_0)^2}{b^2}} + x_0 \quad (4)$$

$$\tan(\Theta) \frac{dz}{dx} \Big|_{(y=y_0, x=x_{surf})} = \pm \frac{b^2(x-x_0)}{a^2 \sqrt{b^2 - \frac{b^2(x-x_0)^2}{a^2}}} \quad (5)$$

Because the ellipsoid has two solutions for each spatial dimension, points below the center of the droplet in the X-direction are mirrored to the other side as: $x = 2\bar{x} - x$ when $x < \bar{x}$. Thus, only one half of the droplet is fitted in the X-dimension. However, the ellipsoid is symmetric in X-Y and due to the mirrored points, all samples are considered. The intersection of the ellipsoid and slab surface x_{surf} is obtained through (4). When deriving the slope as the $\tan(\Theta)$ of the ellipsoid at $y = y_0$ and $x = x_{surf}$ (5), we obtain two solutions, one for contact angles larger than 90° when $z_{surf} > z_0$ and one for contact angles

lower 90° when $z_{surf} < z_0$. (f) Once all frames have been processed, the WCA raw data is fitted by an exponential decay function to obtain an equilibrium reading (6).

$$y = a_0 \exp(-a_1 x) + a_2 \quad (6)$$

3. Results

3.1. Theoretical Modelling

3.1.1. Isolated PHMB Oligomer

We performed molecular dynamic simulations of an isolated PHMB₉ oligomer in explicit water for over 600 ns. The polymer keeps traversing continuously between high and low R_{gyr} states (Figure 1) over the course of the trajectory. Intermediate compact states are stabilized by electrostatic stacking of oppositely charged carbon and nitrogen atoms within the biguanidine groups. Often, these positively charged biguanides are bridged by chloride ions. However, the polymer was easily able to unfold under the conditions of the simulation at ambient temperature and no significant energy barriers were observed by Boltzmann inversion of state probabilities, using the R_{gyr} as the reaction coordinate (Figure 1, insert). Given the cumulative average is beginning to approach a constant value near the end of the simulation, sufficient convergence of the MDS can be assumed.

3.1.2. PHMB Micelle Model

Artificial, brush-like structures were constructed as cutouts from hypothetical micelles, out of linear PHMB oligomers into periodic building blocks. The MD simulation of this building block showed convergence after a few nanoseconds of relaxation as seen by the average R_{gyr} (Figure 2), and the brush-like structure remained stable over the course of the trajectory. The individual oligomers remain closely packed in an extended conformation and the structure incorporates high amounts of chloride ions that bridge and shield the positive charges of the biguanidine groups, as observed during the self-folding process of PHMB. The average and individual R_{gyr} values did not dip below 3 nm, which is in strong contrast to isolated PHMB₉ strands, that always adopted lower values (Figure 1). Due to anisotropic NPT conditions during the relaxation MDS, the obtained structure fits seamlessly in all spatial dimensions and was used to create larger PHMB surface models.

3.1.3. Simulated Water Contact Angles

Simulations on the WCA of variously pentanol-coated titanium dioxide slabs were run for about 20 ns. During the simulations, the initial water cube quickly relaxed into a sphere with sparse surface contact. The contact surface area between the water droplet and the underlying surface slab increased until reaching equilibrium, similar to Figure 4A (right to left). The resulting trajectory was analyzed over time by an automated 3D ellipsoid fit. Due to the mentioned relaxation process, the obtained readings for the WCA over time usually range from a large angle of about 150° at the beginning of the simulation, to lower values down to the boundary of spreading and this depends on the hydrophobicity of the slab. The equilibrium contact angle was obtained by fitting an exponential decay function to the raw data (Figure A1). For this fit, a weighting based on X^2 was applied, which conveniently ignores the initial collapse of the water cube, looking for contact with the surface, without the need for the arbitrary exclusion of data. For higher contact angles, where less overall decay takes place, higher weighting up to X^6 revealed reasonable results (Figure A1).

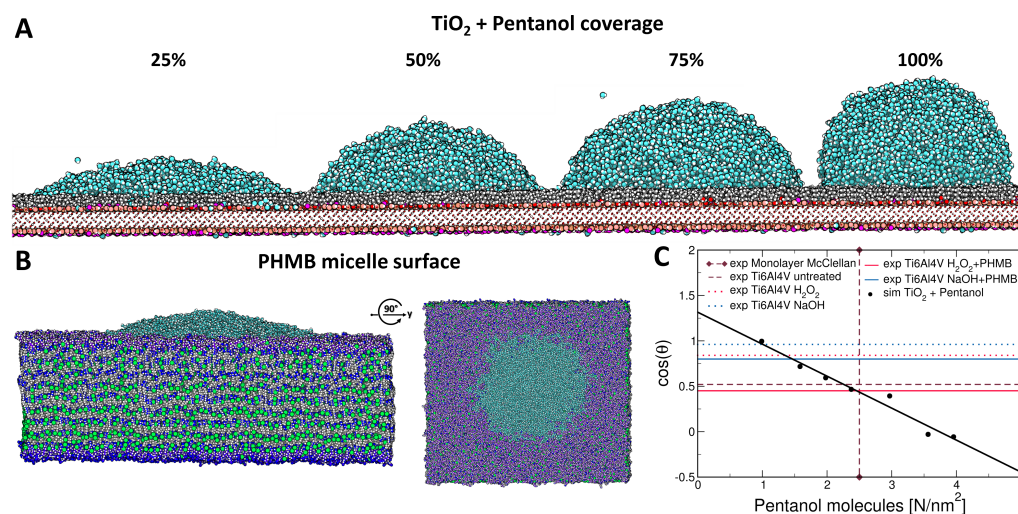


Figure 4. (A) Snapshots near the end of water contact angle simulations on TiO₂ slabs with increasing pentanol coverage. The percentages of 25%, 50%, 75% and 100%, denote the coverage remaining, after randomly removing pentanol molecules from the simulated equilibrium coverage and this assigns to 0.99, 1.98, 2.97 and 3.96 pentanol molecules per nm², respectively. The titanium dioxide crystal is represented by smaller atoms (O: red; Ti: pink). Hydroxylation groups and sodium ions on the top and bottom interfaces are drawn as bigger atoms (O: orange; H: white; Na⁺: magenta). The pentanol molecules (C: grey; O: red) sit on top of the TiO₂ surface with their OH[−] group pointing downwards. The water droplet on top (O: cyan), builds different contact angles with the slab and this depends strongly on the hydrocarbon contamination level. (B) (left) Illustrative snapshot of WCA simulations on pure PHMB surfaces as excerpts of larger micelles with brush-like aggregation of polymer strands. The PHMB oligomers (C: grey; N: blue; Cl[−]: green) stand upright with the PHA and PHT end-groups at the bottom and top, respectively. To differentiate the end-groups visually from the main chain repeat PHM, the carbon atoms of PHA and PHT are colored in different purple shades. (right) Top view. (C) Results from simulated WCA on pentanol-coated titanium dioxide slabs in comparison to experimentally derived contamination levels [39] and wetting properties obtained in vitro in our study. A linear regression $y = 1.3156 - 0.35209x$ yields $R^2 = 0.97$.

The intersection of experimental WCA of untreated, air exposed TiO₂ and a monolayer [39] reading of pentanol fall nicely within the data obtained from molecular dynamics simulations (Figure 4C). As expected, the cosine of the contact angles over the pentanol coverage as molecules per nm² follows a linear relationship with high $R^2 = 0.97$, indicating high accuracy of the overall methodology. We obtained values higher than 93° for very high hydrocarbon contaminations and values in the range of 50°–60° for medium amounts of pentanol coverage. With only slight contamination, lower values near the boundary of spreading occur, which is expectable due to the hydrophilic nature of the underlying titanium oxide crystal.

Similarly, simulations on the wetting properties of PHMB surface models were performed. Stable droplets were observed with no deformation or indent of the polymer slabs. Water molecules did not incorporate significantly into the micelle structure. Only low WCA were obtained, mostly regardless of the PHMB end-group or interface. For the brush-like micelle models, with the two end-groups cyanoguanidine (PHA) and amino (PHT) at their interface, values of 15° and 12° were measured, respectively (Figure 4B). Another model was representing a flat, multilayered stacking of the polymer chains. Here, the water droplet is in contact with the alternating hydrophobic hexamethylene and hydrophilic biguanidine structures and this resulted in a WCA of 11° in our simulation.

3.2. In Vitro Experiments

3.2.1. Carbon Contamination and Water Contact Angle

The measurement of wetting properties indicates a decrease of the WCA due to treatment of the surface with NaOH and H₂O₂ ($16.9^\circ \pm 15.8$; $33.3^\circ \pm 30.1$) in comparison to the untreated specimen surface (58.6 ± 12.6). However, the standard deviation is high for both treatments. The WCA is rising slightly when the surface is coated with PHMB. The NaOH-PHMB (NP) surface has a WCA of $36.8^\circ \pm 5.9$ while the H₂O₂-PHMB (HP) surface has a WCA of $63.0^\circ \pm 4.8$ (Figure 5). The amount of carbon on the surfaces also rose when pre-treated specimens were coated with PHMB. In contrast to the WCA, the carbon contamination on untreated surfaces is similar to the NaOH pre-treated surface. A lower carbon amount accounts for a higher oxygen content on the surface. While the untreated and NaOH pre-treated surfaces only have low carbon contaminations, their oxygen content is high ($48.1^\circ \pm 4.7$ and $48.4^\circ \pm 0.9$). In contrast, high carbon contents on the H₂O₂-PHMB and the NaOH-PHMB surfaces led to decreasing amounts of oxygen on their surface ($25.3^\circ \pm 0.1$ and $26.8^\circ \pm 0.4$) (Figure 5).

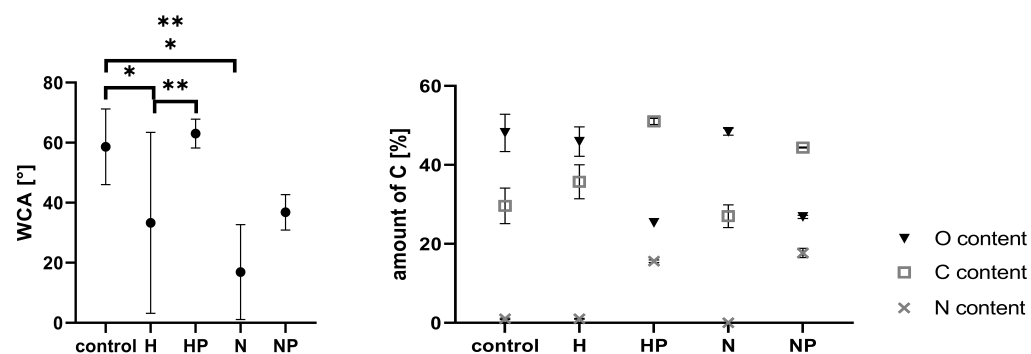


Figure 5. WCA and amounts of carbon, nitrogen and oxygen on Ti6Al4V surface after treatment with NaOH, H₂O₂, and PHMB, respectively. Treatment of the surfaces with NaOH and H₂O₂ led to a significant reduction of WCA. Adsorption of PHMB and possible carbon contaminations led to increasing WCA. The carbon content was highest for the H₂O₂-PHMB (HP) surface, while exhibiting the lowest amounts of nitrogen and oxygen. The lowest carbon content was reached after treatment of the surface with NaOH. * $p < 0.05$, ** $p < 0.01$, *** $p < 0.001$.

3.2.2. Ti6Al4V Surface Treatment with NaOH or H₂O₂ and Resulting Biguanide Adsorption

PHMB adsorption on polished surfaces pre-treated with H₂O₂ (24 h), led to adsorption of 2–4 µg/specimen PHMB. Cb surfaces treated with H₂O₂ adsorbed 6–8 µg/specimen PHMB. Increasing amounts of PHMB were adsorbed (about 18–23 µg/specimen) onto the surface of a NaOH-processed Ti6Al4V specimen by incubation in 30 µg/mL PHMB for 24 h, but there were no differences between p- and cb-Ti6Al4V discs (Figure 6). Staining of PHMB adsorbed at the NaOH pre-treated specimen surface was carried out using Rose Bengal, resulting in a clear, visible and permanent coloration (Figure 6). The PHMB on H₂O₂ pre-treated surfaces was also stained with the same technique, but did not result in coloration visible to the naked eye. But, when H₂O₂ pre-treated specimens were incubated in a solution containing 6% PHMB, via stereomicroscopy, isle-like spots of Rose Bengal staining were visible (Figure 7).

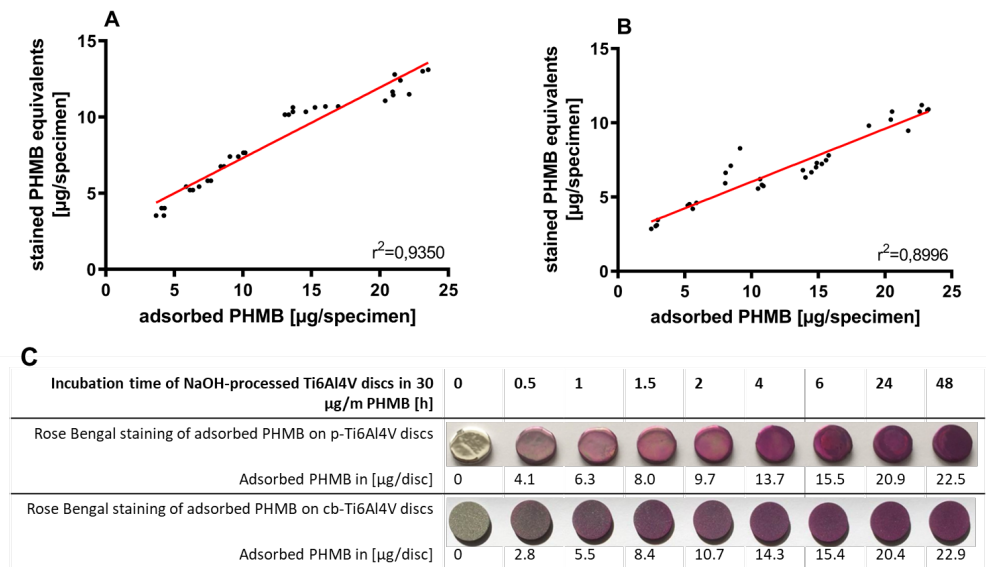


Figure 6. PHMB adsorption after incubation of test specimen in 5M NaOH at 60 °C and staining with Rose Bengal for 20 h. The amount of bound PHMB is rising with increasing incubation time in the PHMB solution but is not dependent on surface roughness. (A) PHMB adsorption on polished test specimen, incubated in NaOH for 2 h before. (B) PHMB adsorption on corundum-blasted test specimens incubated in NaOH for 1 h before. (C) Amounts of adsorbed PHMB [$\mu\text{g}/\text{specimen}$] of NaOH-processed p- and cb-Ti6A4V discs after different incubation times in 30 $\mu\text{g}/\text{mL}$ PHMB-coating solution and the corresponding Rose Bengal-stained surfaces to monitor PHMB.

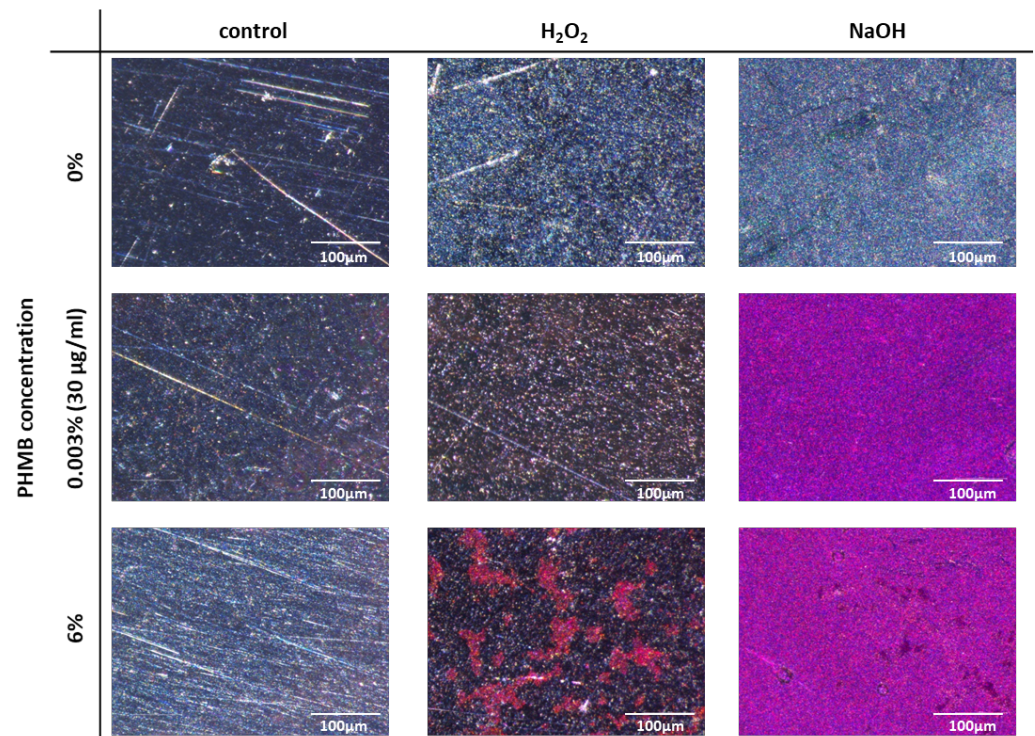


Figure 7. PHMB stained with Rose Bengal after treatment of the test specimen with NaOH and H_2O_2 following coating with PHMB in 30 $\mu\text{g}/\text{mL}$ (0.003%) or 6% PHMB solution. Staining of the adsorbed PHMB was possible on NaOH pre-treated surfaces. The treatment with H_2O_2 following PHMB adsorption (30 $\mu\text{g}/\text{mL}$) did not result in a visible staining. Treatment with 6% PHMB enabled a staining of single islands of PHMB.

Regarding the calculated amounts of Rose Bengal consumption, and thus, the stained PHMB equivalents, there is a clear correlation to the amount of adsorbed PHMB measured and calculated after spectrophotometry. This correlation is also visible on the stained NaOH-PHMB coated test specimens. Binding of CHG on polished test specimens was conducted over various periods of time. The amount of bound CHG increased as a function of time (Figure A2). The process of coating is comparable to the reaction of NaOH-treated surfaces with PHMB [9]. After incubation of the specimen in CHG solution for 2 h, the amount of adsorbed CHG was about 9.64 ± 0.11 $\mu\text{g}/\text{specimen}$. Similar amounts of PHMB were absorbed on the specimens after the same incubation period. Longer incubation in PHMB solution led to higher amounts of adsorption, whereas longer incubation in CHG solution resulted in no significant increase in mass coverage.

3.2.3. Staining of Anionic Equivalents

Staining and calculation of anionic equivalents with TBO showed more anionic groups on H_2O_2 - and NaOH-processed surfaces than on untreated control specimens. Additionally, specimens with Hellmanex III-cleaned surface were stained with TBO and revealed a slight increase in anionic equivalents on the surface in contrast to uncleaned surfaces. The amount of anionic equivalents on H_2O_2 -treated surfaces rose 11.6-fold and after NaOH-processing, resulted in an 18.7-fold increase compared to the untreated control.

3.2.4. Adsorption of FITC-PHMB on Test-Specimen

FITC-PHMB solution containing 30 $\mu\text{g}/\text{mL}$ PHMB-equivalents was used for coating untreated p-Ti6Al4V discs (control, 24 h), H_2O_2 -oxidized specimens (24 h), and NaOH-treated specimens (2 h). FITC was bound to the amino group of PHMB and, thus, blocks adsorption via this end-group. On the untreated specimen, some minor fluorescent FITC-PHMB spots were visualized (Figure A3). After H_2O_2 treatment and NaOH processing of p-Ti6Al4V specimens, FITC-PHMB can be monitored over the whole surface. NaOH pre-treated specimens showed slightly higher fluorescence than the specimens with H_2O_2 oxidized surfaces.

3.2.5. SEM Showed Differences in Surface Texture

Polished control specimens, as well as NaOH- and H_2O_2 -treated specimens without and with PHMB coating, were analysed via SEM. Two different magnifications were displayed. The surface of control specimens is very even. In contrast, treatment with H_2O_2 led to formation of island-shaped areas (Figure 8). The coating with PHMB did not result in a change of this appearance. The NaOH treatment led to a clear difference in the surface appearance. Instead of island-shaped single areas, the whole surface had a network-like texture.

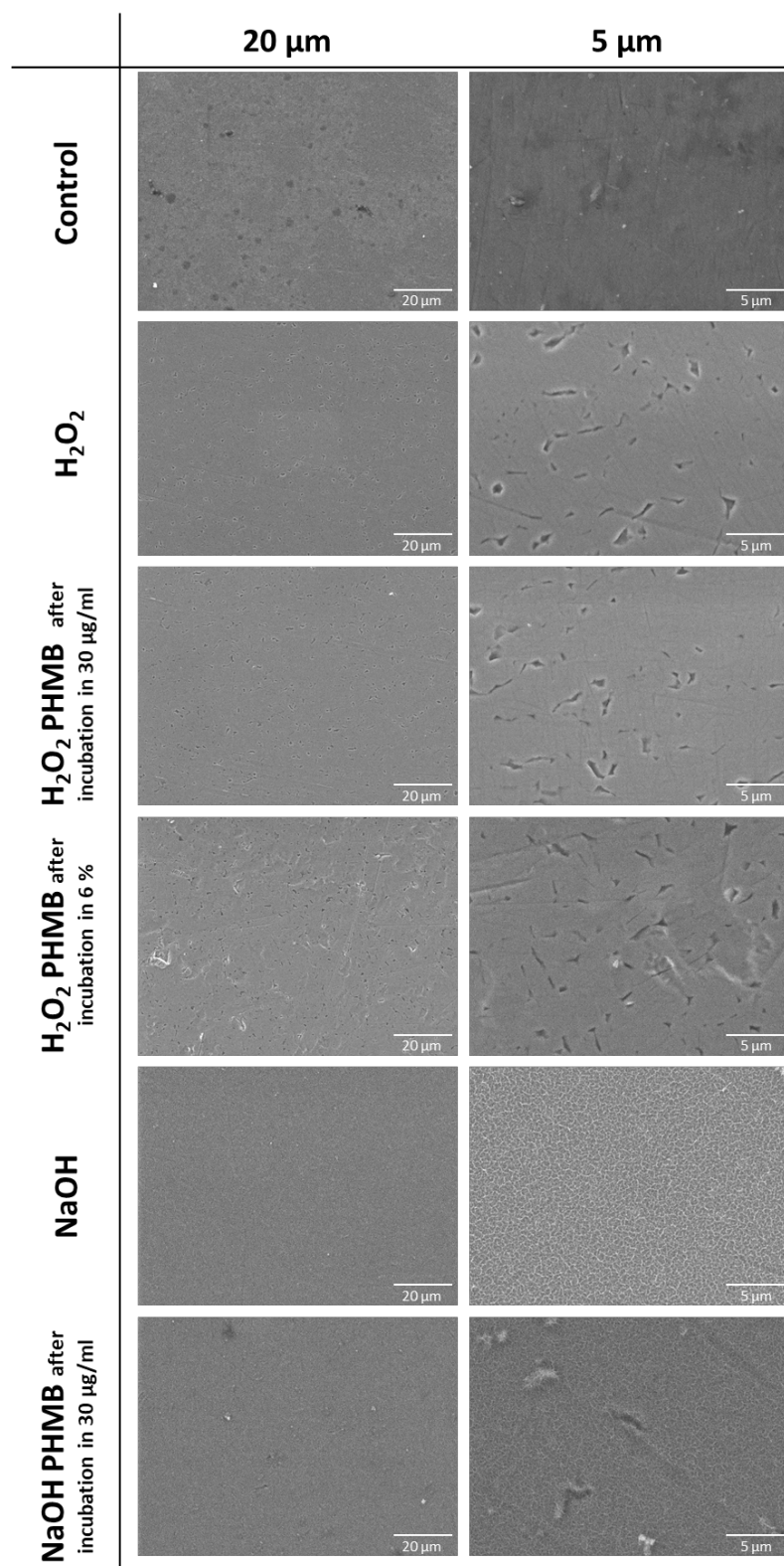


Figure 8. Surface characteristics of differently treated Ti6Al4V surfaces. Untreated Ti6Al4V specimens show an even surface. Treatment with H₂O₂ led to the formation of an isle-like structure. The NaOH treatment resulted in a quite different pattern, that can be described as network-like. Adsorption of PHMB had no influence on surface structure visible with SEM.

3.2.6. Cell Viability, Activity of Alkaline Phosphatase and Calcium Apatite Formation

Cell viability of SaOs-2 cells after a 7 day cell culture on NaOH pre-treated Ti6Al4V surfaces rose to 112% in comparison to control test specimen. Viability on PHMB-coated surfaces (2 h, 10 μg) further rose to 120%. The cell viability on PHMB-coated specimens with 18–23 μg (20 h) was comparable to the viability on NaOH pre-treated surfaces (113%; data not shown). In contrast to rising cell viability observed after 7 days of cell culture (as a result of surface treatment), and independently of amount of adsorbed PHMB, higher amounts of PHMB (20 h) led to decrease in ALP activity as well as CaP formation (Figure 9). Amounts of 10 μg PHMB and NaOH pre-treated surfaces led to slight increases in both ALP activity and CaP formation.

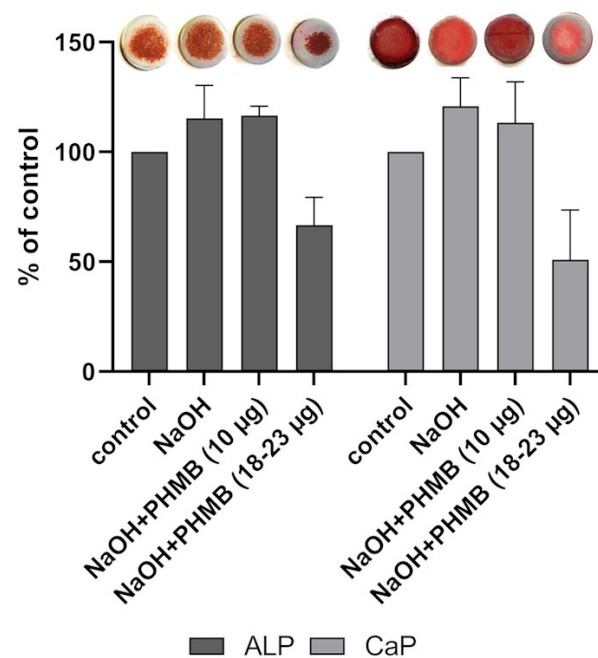


Figure 9. Staining of alkaline phosphatase and calcium apatite after 7 day culture of SaOs-2 osteoblasts on Ti6Al4V specimens with different amounts of adsorbed PHMB. Higher amounts of PHMB led to a decreased formation of calcium apatite and a lower activity of alkaline phosphatase in comparison to untreated surfaces. Treatment with NaOH alone, and with low amounts of PHMB (10 μg), had slightly increasing effects on ALP and CaP formation.

4. Discussion

4.1. Structure and Effect of PHMB

The polycationic polymeric PHMB consists of alternating hydrophilic and hydrophobic segments enabling an adsorption onto negatively charged surfaces [11]. DePaula et al. stated that this special amphiphile structure of PHMB leads to the formation of “single-molecule-micelles” in water [37]. However, in contrast to a typical surfactant micelle, the PHMB micelle is formed of the segments of the polymer chain instead of adjacent single molecules [37]. This consideration was proven and claimed confirmed by dePaula et al. using DLS measurements that revealed a sudden change in particle size, depending on the PHMB concentration in solution [37]. Small particles (size of 0.5–10 nm in diameter) were found for high PHMB concentrations of about 10^{-1} M and larger aggregates (size about 1000 nm) were observed for lower concentrations up to 10^{-6} M. The critical micelle concentration was determined to 5×10^{-2} mol/dm⁻³ [37].

Until recently, the mode of action of PHMB was ascribed to its polycationic properties that result in damage of microbial plasma membranes, as phospholipids are of opposite charge. PHMB adsorption damages the membranes, leading to leakage of cell organelles and finally cell death [40,41]. Atomistic molecular dynamic studies of Zaki et al. revealed

that polyelectrolytes self-assemble into an ordered structure, a behavior that is especially observed in polyelectrolytes with a low charge density. They pointed out, that PHMB can also self-assemble into small nano-like hairpin structures as seen for other biological polyelectrolytes, enabling cell penetration [42]. These data are in accordance with the DLS measurement of dePaula et al. because both groups were able to show an aggregation of PHMB in solution [37,42]. Thus, they hypothesize a mode of action different to the current belief: PHMB nano-objects interact with the lipid membrane and enter the cell without perforation or disruption of the membrane. This kind of entry was also observed for cationic nanoparticles (cNP) that enter a cell via direct translocation [43]. Later, this mechanism was confirmed for PHMB by Chindera et al. (2016). By using light and fluorescence microscopy, they did not find lysed cells or cells with membrane damage after PHMB treatment, although PHMB was located in the cytoplasm. Additionally, Chindera et al. revealed an arrest in cell division after PHMB treatment and a condensation of bacterial chromosomes. In contrast, in mammalian cells, PHMB is excluded from the nuclei due to capture in vesicles. Furthermore, an interaction of PHMB with membrane proteins was demonstrated by Sowlati-Hashjin et al. via atomistic molecular dynamic simulations, they revealed an attachment of PHMB to the surface of a phospholipid bilayer due to its cationic charge and its resulting electrostatic interaction with the phospholipid headgroups. Consequently, the molecules partially penetrate the membrane without any perforation or disruption, and finally enter the cell by binding mechanisms with the membrane lipids [44]. Sowlati-Hashjin et al. also analyzed the interplay of PHMB with DNA, hypothesizing that the interaction results in inhibition of DNA replication processes.

4.2. Simulated Wetting Properties

To understand the influence of the surface treatment on the PHMB adsorption and the resulting effects on the wetting properties, molecular dynamic simulations were conducted to show whether alternative interfaces of the PHMB coating could lead to significantly different water contact angles, as observed for the H₂O₂ and NaOH treatments in vitro. This shall show if PHMB binds in a different manner with respect to the pre-treatment of specimen and could also explain the variance in the observed mass coverage between both treatments. We assumed, if there is a special PHMB binding mode that may influence the wetting properties of the specimen after adsorption, it may largely consist of the same micelle-like substructure that the aggregates of this polymer are suspected to adopt. Thereby, binding of only specific end-groups of the polymer would clearly restrict the mass coverage of the coating, just by the surface area of the specimen and the density of binding sites on that surface. In this case, we expect a high influence of surface roughness. However, in case of the polymer stacks up in multiple amorphous layers, a much higher mass coverage would be feasible and effects of surface roughness should be negligible.

According to a previous study [8], when dissolved, isolated PHMB oligomers tend to reduce their solvent accessible surface area (SASA) and radius of gyration (R_{gyr}) by self aggregation of biguanide groups and thereby fold into compact states. However, multiple molecules tend to more linear conformations and out chain aggregates. Thus, shielding of the solvent-exposed surface area can occur with less need for internal deformation of oligomers and are thus revealed to be energetically more favorable [8].

In this study, long MD simulations of single PHMB oligomers did also not point out distinct folding states and rather resulted in a broad range of low R_{gyr} structures in the range of 1 nm (Figure 1). According to dePaula et al. [37], PHMB in aqueous solution occurs in either large aggregates of around 1 μ m or very small entities of 1 nm as observed by DLS over increasing PHMB concentrations. We conclude that in a concentration regime beyond the critical micelle concentration (CMC), PHMB occurs mostly as isolated monomers, considering the radius of gyration from MDS being in the range of the hydrodynamic diameter obtained by DLS. Our PHMB micelle model therefore assumes a typical brush-like structure [45], were PHMB oligomers are maximally extended and stacked. This

substructure was used to construct artificial surfaces, that allowed the simulation of water contact angles on pure PHMB on various interfaces.

Simulations on the wetting properties, in terms of WCA, were performed for pure PHMB and for differently pentanol-coated titanium oxide surfaces, as a contamination model. An automated measurement of contact angles from simulation was implemented by means of accurate 3D ellipsoid fits, that resembled the increasing hydrophobicity with increasing coverage of TiO₂ with hydrocarbons. The medium contamination coverage of 2.5 pentanol molecules per nm² we obtained from the simulations is in line with experimentally derived monolayers. The corresponding WCA of about 63° falls in the range of the untreated Ti6Al4V discs. These data suggest that PHMB is unlikely to increase the hydrophobicity of the specimen significantly. With values in the range of 11° to 15° degrees, pure PHMB reveals as hydrophilic as a rather freshly cleaned specimen, but saturation with PHMB can potentially block off contamination. In contrast, the WCA obtained from pentanol coated titanium slabs, indicate that hydrocarbon contamination is likely the major driving factor for the changes in wetting properties.

4.3. Effects of Surface Treatment on Adsorption

PHMB is a micobicial agent consisting of repeating hexamethylene biguanide units, terminated with different end-groups. The guanidino end-group accounts for 70.3% of the end-groups, 16.5% of the end-groups are amino groups whereas 13.2% are cyanoguanidine groups [46]. The most abundant combination is a molecule with one cyanoguanidine and one amino group [16]. Similar in structure to PHMB is CHG, which also has an antimicrobial effect against various microorganisms, but only consists of one hexamethylene biguanide group terminated by p-chlorophenyl rests. In contrast to PHMB, an adsorption of CHG to a surface is not possible via these end-groups. However, both molecules adsorb at the specimens surface in similar amounts after 2 h of incubation. In addition, blocking of the amino group of PHMB with FITC did not suppress the ability of PHMB adsorbing to the Ti6Al4V surface. The positive charge of PHMB is located at the hexamethylene biguanide units, enabling the molecule to interact with the anionic charges generated by surface pre-treatment. With rising anionic groups, rising amounts of PHMB were adsorbed. Therefore we conclude that an adsorption of PHMB or CHG happens mainly with the hexamethylene biguanide units, due to their cationic charge. However, the adsorption generally has to be enabled by a surface treatment beforehand, to generate anionic charges and remove contamination.

As revealed by SEM investigations, the surface morphology produced by NaOH treatment differs significantly from that obtained by H₂O₂ treatment. The latter results in an even surface with some etching pits whereas the reaction in 5 M NaOH generates a network-like texture presumably constructed of TiO₂ units. This surface change on the microscale might contribute to the considerably higher PHMB adsorption observed at NaOH treated Ti6Al4V test specimens in comparison to Ti6Al4V samples prepared with H₂O₂. Both, the H₂O₂ and the NaOH treatment of the Ti6Al4V surface led to the generation of anionic groups and both treatments resulted in strongly reduced WCA. The formation of anionic groups on the surface enables a fast contamination with hydrocarbons, resulting in a higher carbon content in comparison to the control surface. However, the carbon content on NaOH-PHMB coated surfaces is lower than that for the H₂O₂-PHMB surface. This may arise from the formation of isle-like areas after H₂O₂ treatment in contrast to NaOH treatment, that resulted in an evenly modified surface. Comparing NaOH-PHMB and H₂O₂-PHMB surfaces, the NaOH-PHMB specimens exhibit a higher nitrogen content on their surface, while possessing lower amounts of carbon, confirming that NaOH pre-treatment leads to higher amounts of adsorbed PHMB and partially preventing a further carbon contamination. This presumption is supported by a rising C:N-proportion of the NaOH-PHMB coated surface (3.3) in comparison to the H₂O₂-PHMB surface (2.7) as well as pure PHMB (1.6). In summary, one may assume that the surface–after NaOH treatment–can

be covered with PHMB more completely, whereas the H₂O₂ treatment due to the isle-like structure enables only single large micelles adsorption.

Higher PHMB concentrations (6%) result in disruption of the micelles and more single molecules in solution. Only with these high concentrations, a stainable coating of the H₂O₂ treated surface was possible. We believe single molecules can adsorb with higher amounts than larger micelles, because only isles large enough to hold full micelles were able to bind PHMB previously. Now, also smaller isles can capture PHMB from solution and build multilayered aggregates. A stacking and aggregation of PHMB molecules was also shown earlier by MDS of Mueller et al. and was confirmed in the current study by a stable brush-like structure.

4.4. Osseointegration in the Presence and Absence of PHMB Coating

The treatment of Ti6Al4V surfaces with H₂O₂ and NaOH led to a reduction in water contact angles and increased the adsorption of PHMB. Simulated WCA of pure PHMB are in the range of 11°–15°, leading to the assumption, that the higher WCA on PHMB-coated surfaces are mainly the results of carbon contamination [47]. The isle-like structure of H₂O₂ pre-treated and also of H₂O₂-PHMB surfaces may enable a higher adsorption of carbon contaminants than for NaOH-treated surfaces. This is also reflected by the XPS analysis, revealing a higher carbon content for the H₂O₂-PHMB surface than for the NaOH-PHMB surface as well as the H₂O₂- and NaOH pre-treated surfaces alone. High amounts of carbon contamination increase hydrophobicity, whereas higher amounts of oxygen go along with increased hydrophilicity. The NaOH-PHMB surface lies in-between the more hydrophobic H₂O₂-PHMB surface and the more hydrophilic pre-treated surfaces. Hydrophilic surfaces exhibit a higher surface energy and enable a better osseointegration [48] due to binding of fibronectin to cationic charges [49]. Next to the more hydrophilic surface due to NaOH-PHMB coating, PHMB itself enhances this binding possibility due to its cationic charge and a coverage of anionic groups. This also increases the activity of ALP and the amount of CaP, as it was stated by Zhao et al. [4]. The data presented here go along with this predication, since ALP, as well as CaP, are slightly rising on NaOH and NaOH-PHMB surfaces, identifying possible positive effects on osseointegration. However, very high amounts of PHMB on the surface result in a decrease of ALP activity and CaP formation. As Hornschuh et al. revealed, rising amounts of PHMB do not affect cell viability of SaOs-2 osteoblasts until the PHMB amount reaches a specific concentration ($21.06 \pm 0.58 \mu\text{g}$) on the surface, that led to a decrease in cell viability. This confirms the claim that PHMB does not effect cell activity until it reaches a certain amount. Moreover, even if the amount of PHMB is too high and it can have negative effects, the advantage of the NaOH pre-treatment is in the ability to adjust the amounts of bound-PHMB at the surface. While the impact of the PHMB coated surface to osteoblast-like cells is crucial for an estimation of biocompatibility, interactions with the environment surrounding the implant e.g. with further cell types as immune cells, especially monocytes and macrophages, should also be taken into account. For instance, proteins from the surrounding environment can possibly adsorb to the surface influencing osteoblast behaviour as cell attachment, spreading and viability. Immune cells can also attach to the surface, secreting pro- or anti-inflammatory cytokines, thus regulating the healing process after implantation, and also affecting formation of connective tissue possibly leading to fibrous encapsulation. These effects may reduce or enhance the biocompatibility. Therefore, further investigations, especially regarding interactions of the implant surface with monocytes and macrophages, were already undertaken.

4.5. Surface Composition and Influence on PHMB Adsorption

The isle-like formation of PHMB on H₂O₂ treated surfaces led to a surface roughness-dependent adsorption. With increased roughness, more PHMB is adsorbed, because a higher surface area is available. When the cleaned isle-like areas are covered with PHMB, no additional PHMB adsorption is possible. In contrast, the NaOH treatment led to the full coverage of the surface with PHMB as a film. This film is not dependent on the roughness

but presumably enables a stacking of many PHMB molecules, leading to rising amounts of PHMB after prolonged incubation in PHMB solution.

5. Conclusions

We conclude, that a treatment of the Ti6Al4V surface with either NaOH or H₂O₂ is essential for the generation of anionic groups and for the removal of carbon contamination, thus enabling adsorption of PHMB. The treatments led to distinct effects on surface constitution, becoming apparent by an isle-like surface modification in contrast to an evenly modified surface in case of H₂O₂ or NaOH cleaning, respectively. Our MD simulations leave behind the image that the PHMB coating is not a major cause for an increased hydrophobicity of the implant surface, but rather hydrocarbon contamination is. From our perspective, PHMB mainly blocks the hydrophilic sites on the Ti6Al4V implant material and thereby causes a slight increase in the contact angle. The adsorption mechanism is determined by the binding of the cationic PHMB chain to anionic groups on the implant surface, an influence of the end-groups was not shown neither *in vitro* nor *in silico*. The cell viability, as well as ALP activity and CaP formation, are not negatively impaired until a certain amount of PHMB is adsorbed on the surface, leading to good cytocompatibility of the PHMB coating in regard to osteoblast-like cells, including a protecting effect against carbon contamination.

Given our results, for the preparation of Ti6Al4V-based implant materials, a focus should be placed on removing carbon contamination and protecting the surface from capturing new contaminations. This may be especially of interest due to raised concentrations of hydrocarbons in the air of clinical areas, caused by disinfectants. Ultimately, a cleaning procedure including NaOH treatment and subsequent protective and antimicrobial coatings with PHMB may lead to a promising direction to overcome implant-associated complications.

Supplementary Materials: The following are available online at <https://www.mdpi.com/article/10.3390/coatings11091118/s1>.

Author Contributions: Conceptualization, G.M., U.L., C.P., N.G., P.Z. and A.K.; methodology, G.M., N.G. and M.K.; software, N.G. and M.K.; validation, N.G., P.Z., M.K. and G.M.; formal analysis, P.Z. and N.G.; investigation, M.H., T.S., N.G., E.G. and P.Z.; resources, C.P., U.L. and M.D.; data curation, G.M., P.Z. and N.G.; writing—original draft preparation, N.G. and P.Z.; writing—review and editing, M.D., M.K., U.L., G.M., A.K. and M.H.; visualization, N.G. and P.Z.; supervision, G.M.; project administration, G.M.; funding acquisition, G.M., U.L. and C.P. All authors have read and agreed to the published version of the manuscript.

Funding: This work was supported by the Ministry of Economics, Employment, and Health Mecklenburg-Vorpommern in Germany (grant No. TBI-V-1-059-VBW-020).

Institutional Review Board Statement: Not applicable.

Informed Consent Statement: Not applicable.

Data Availability Statement: Data is contained within the article or supplementary material. Further data are available on request.

Acknowledgments: The authors thank Daniel Möller (Biophysical Chemistry Department, Institute of Biochemistry, University Greifswald, Germany) for his contributions on the MD simulations as well as Walter Langel who originally initiated the theoretical investigations for this project as well as Dagmar Jasinski, Birgit Finke and Uwe Lindemann (INP, Greifswald) for competent technical assistance in WCA and XPS measurement and Anne Brandenburg (Institute of Hygiene and Environmental Medicine, University Medicine Greifswald, Germany) for technical assistance in cell culture experiments.

Conflicts of Interest: The authors declare no conflict of interest. The funders had no role in the design of the study; in the collection, analyses, or interpretation of data; in the writing of the manuscript, or in the decision to publish the results.

Appendix A. Supporting Figures

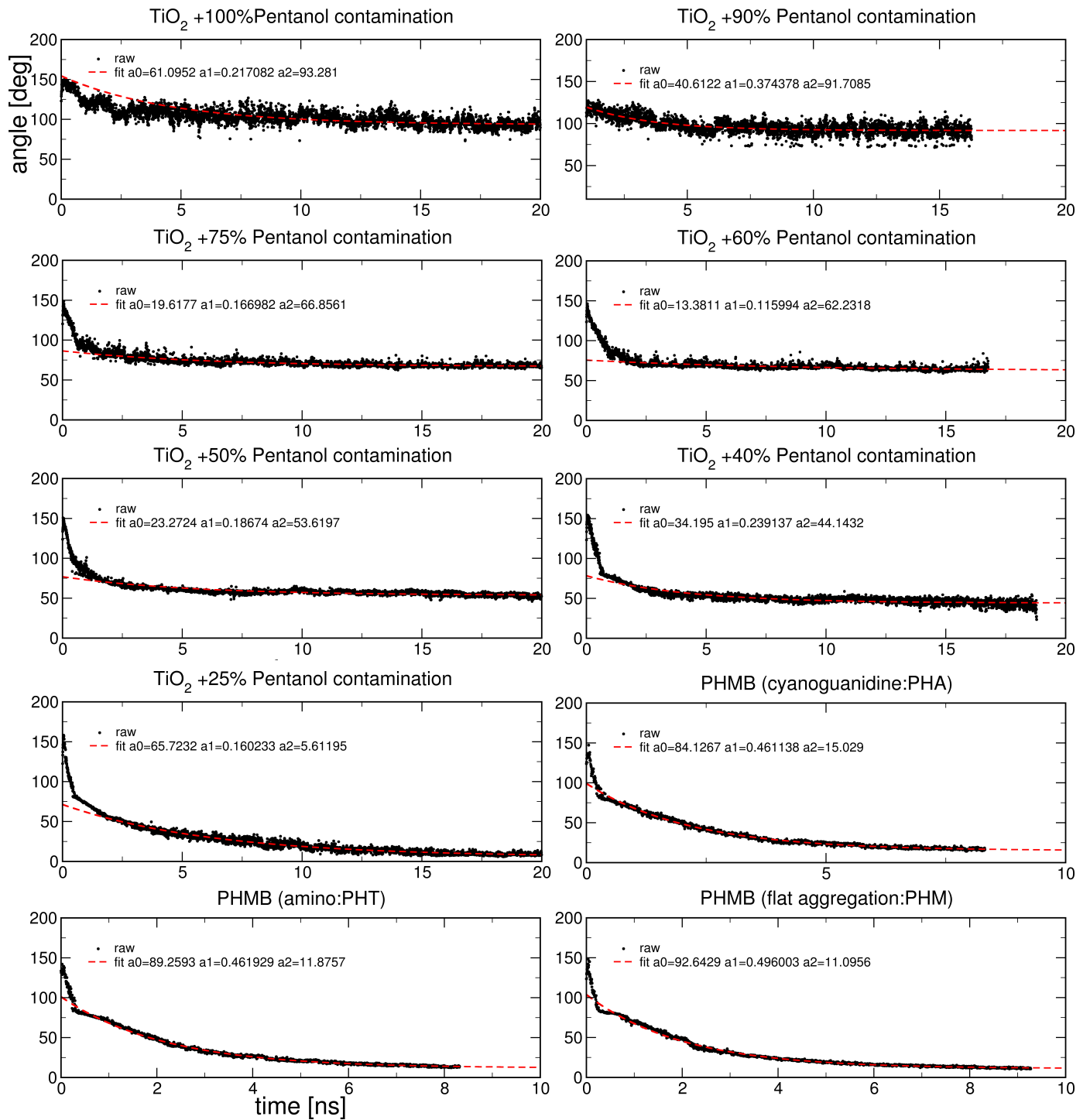


Figure A1. Raw WCA data obtained by novel automated 3D ellipsoid fit procedure and subsequent decay fit.

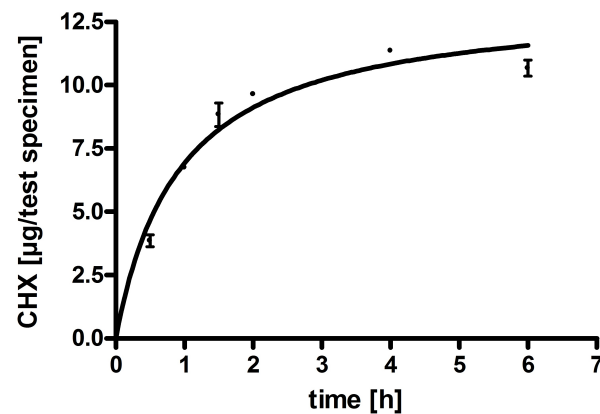


Figure A2. Adsorption of CHG to polished test specimens pre-treated with 5 M NaOH (2 h, 60 °C). Kinetics of adsorption are comparable to adsorption of PHMB to NaOH pre-treated surfaces.

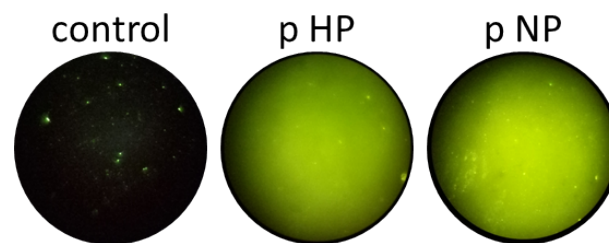


Figure A3. Representative fluorescence microscopic images of adsorbed FITC-PHMB at the untreated surface (control), and after oxidation p-Ti6Al4V discs with H₂O₂ (HP) or after NaOH treatment (NP). Although the amino end-group was blocked with FITC, PHMB adsorbed onto the treated surfaces.

References

- Hierro-Oliva, M.; Gallardo-Moreno, A.M.; Gonzalez-Martin, M.L. XPS Analysis of Ti6Al4V Oxidation Under UHV Conditions. *Metall. Mater. Trans. A* **2014**, *45*, 6285–6290. [[CrossRef](#)]
- Da Fonseca, C.; Boudin, S.; da Cunha Belo, M. Characterisation of titanium passivation films by in situ ac impedance measurements and XPS analysis. *J. Electroanal. Chem.* **1994**, *379*, 173–180. [[CrossRef](#)]
- Kang, B.S.; Sul, Y.T.; Oh, S.J.; Lee, H.J.; Albrektsson, T. XPS, AES and SEM analysis of recent dental implants. *Acta Biomater.* **2009**, *5*, 2222–2229. [[CrossRef](#)]
- Zhao, G.; Schwartz, Z.; Wieland, M.; Rupp, F.; Geis-Gerstorf, J.; Cochran, D.L.; Boyan, B.D. High surface energy enhances cell response to titanium substrate microstructure. *J. Biomed. Mater. Res. Part A* **2005**, *74A*, 49–58. [[CrossRef](#)]
- Lim, Y.J.; Oshida, Y. Initial contact angle measurements on variously treated dental/medical titanium materials. *Bio-Med. Mater. Eng.* **2001**, *11*, 325–341.
- Sakai, N.; Fukuda, K.; Shibata, T.; Ebina, Y.; Takada, K.; Sasaki, T. Photoinduced Hydrophilic Conversion Properties of Titania Nanosheets. *J. Phys. Chem. B* **2006**, *110*, 6198–6203. [[CrossRef](#)]
- Dhaliwal, J.; David, S.; Zuhlilmi, N.; Dhaliwal, S.; Knights, J.; Junior, R. Contamination of titanium dental implants: A narrative review. *SN Appl. Sci.* **2020**, *2*, 1011. [[CrossRef](#)]
- Müller, G.; Benkhail, H.; Matthes, R.; Finke, B.; Friedrichs, W.; Geist, N.; Langel, W.; Kramer, A. Poly (hexamethylene biguanide) adsorption on hydrogen peroxide treated Ti–Al–V alloys and effects on wettability, antimicrobial efficacy, and cytotoxicity. *Biomaterials* **2014**, *35*, 5261–5277. [[CrossRef](#)]
- Hornschuh, M.; Zwicker, P.; Schmidt, T.; Finke, B.; Kramer, A.; Müller, G. Poly (hexamethylene biguanide), adsorbed onto Ti–Al–V alloys, kills slime-producing Staphylococci and Pseudomonas aeruginosa without inhibiting SaOs-2 cell differentiation. *J. Biomed. Mater. Res. Part Appl. Biomater.* **2019**, *108*, 1801–1813. [[CrossRef](#)] [[PubMed](#)]
- Groll, J.; Fiedler, J.; Bruellhoff, K.; Moeller, M.; Brenner, R.E. Novel Surface Coatings Modulating Eukaryotic Cell Adhesion and Preventing Implant Infection. *Int. J. Artif. Organs* **2009**, *32*, 655–662. [[CrossRef](#)] [[PubMed](#)]
- Kramer, A.; Eberlein, T.; Müller, G.; Dissemond, J.; Assadian, O. Re-evaluation of polihexanide use in wound antisepsis in order to clarify ambiguities of two animal studies. *J. Wound Care* **2019**, *28*, 246–255. [[CrossRef](#)] [[PubMed](#)]
- Hornschuh, M.; Zwicker, P.; Schmidt, T.; Kramer, A.; Müller, G. In vitro evaluation of contact-active antibacterial efficacy of Ti–Al–V alloys coated with the antimicrobial agent PHMB. *Acta Biomater.* **2020**, *106*, 376–386. [[CrossRef](#)] [[PubMed](#)]
- Tengvall, P.; Elwing, H.; Sjöqvist, L.; Lundström, I.; Bjursten, L. Interaction between hydrogen peroxide and titanium: A possible role in the biocompatibility of titanium. *Biomaterials* **1989**, *10*, 118–120. [[CrossRef](#)]

14. Köppen, S.; Langel, W. Simulation of the interface of (100) rutile with aqueous ionic solution. *Surf. Sci.* **2006**, *600*, 2040–2050. [[CrossRef](#)]
15. Friedrichs, W.; Langel, W. Atomistic modeling of peptide adsorption on rutile (100) in the presence of water and of contamination by low molecular weight alcohols. *Biointerphases* **2014**, *9*, 031006. [[CrossRef](#)]
16. O'Malley, L.P.; Hassan, K.Z.; Brittan, H.; Johnson, N.; Collins, A.N. Characterization of the biocide polyhexamethylene biguanide by matrix-assisted laser desorption ionization time-of-flight mass spectrometry. *J. Appl. Polym. Sci.* **2006**, *102*, 4928–4936. [[CrossRef](#)]
17. Bratt, H.; Hathway, D.E. Characterization of the urinary polymer-related material from rats given poly[biguanide-1,5-diylhexamethylene hydrochloride]. *Die Makromol. Chem.* **1976**, *177*, 2591–2605. [[CrossRef](#)]
18. Sano, S.; Kato, K.; Ikada, Y. Introduction of functional groups onto the surface of polyethylene for protein immobilization. *Biomaterials* **1993**, *14*, 817–822. [[CrossRef](#)]
19. Gilbert, P.; Pemberton, D.; Wilkinson, D.E. Synergism within polyhexamethylene biguanide biocide formulations. *J. Appl. Bacteriol.* **1990**, *69*, 593–598. [[CrossRef](#)]
20. Gilbert, P.; Pemberton, D.; Wilkinson, D.E. Barrier properties of the Gram-negative cell envelope towards high molecular weight polyhexamethylene biguanides. *J. Appl. Bacteriol.* **1990**, *69*, 585–592. [[CrossRef](#)]
21. Chindera, K.; Mahato, M.; Sharma, A.K.; Horsley, H.; Kloc-Muniak, K.; Kamaruzzaman, N.; Kumar, S.; Mcfarlane, A.; Stach, J.; Bentin, T.; et al. The antimicrobial polymer PHMB enters cells and selectively condenses bacterial chromosomes. *Sci. Rep.* **2016**, *6*, 23121. [[CrossRef](#)] [[PubMed](#)]
22. Schaftenaar, G.; Vlieg, E.; Vriend, G. Molden 2.0: Quantum chemistry meets proteins. *J. Comput. Aided Mol. Des.* **2017**, *31*, 789–800. [[CrossRef](#)]
23. Frisch, M.J.; Trucks, G.W.; Schlegel, H.B.; Scuseria, G.E.; Robb, M.A.; Cheeseman, J.R.; Montgomery, J.A., Jr.; Vreven, T.; Kudin, K.N.; Burant, J.C.; et al. *Gaussian 03, Revision C.02*; Gaussian, Inc.: Wallingford, CT, USA, 2004.
24. Bayly, C.I.; Cieplak, P.; Cornell, W.; Kollman, P.A. A well-behaved electrostatic potential based method using charge restraints for deriving atomic charges: The RESP model. *J. Phys. Chem.* **1993**, *97*, 10269–10280. [[CrossRef](#)]
25. Case, D.; Ben-Shalom, I.; Brozell, S.; Cerutti, D.; Cheatham, T., III; Cruzeiro, V.; Darden, T.; Duke, R.; Ghoreishi, D.; Gilson, M.; et al. *AMBER 2018*; University of California: San Francisco, CA, USA, 2018.
26. Case, D.A.; Darden, T.A.; Cheatham, T.E., III; Simmerling, C.L.; Wang, J.; Duke, R.E.; Luo, R.; Crowley, M.; Walker, R.C.; Zhang, W.; et al. *AMBER 10*; University of California: San Francisco, CA, USA, 2008.
27. Wang, J.; Wolf, R.M.; Caldwell, J.W.; Kollman, P.A.; Case, D.A. Development and testing of a general amber force field. *J. Comput. Chem.* **2004**, *25*, 1157–1174. [[CrossRef](#)]
28. Phillips, J.C.; Hardy, D.J.; Maia, J.D.C.; Stone, J.E.; Ribeiro, J.V.; Bernardi, R.C.; Buch, R.; Fiorin, G.; Hénin, J.; Jiang, W.; et al. Scalable molecular dynamics on CPU and GPU architectures with NAMD. *J. Chem. Phys.* **2020**, *153*, 044130. [[CrossRef](#)]
29. NVIDIA; Vingelmann, P.; Fitzek, F.H. CUDA. Release: 10.2.89. 2020.
30. Essmann, U.; Perera, L.; Berkowitz, M.L.; Darden, T.; Lee, H.; Pedersen, L.G. A smooth particle mesh Ewald method. *J. Chem. Phys.* **1995**, *103*, 8577–8593. [[CrossRef](#)]
31. Hopkins, C.W.; Grand, S.L.; Walker, R.C.; Roitberg, A.E. Long-Time-Step Molecular Dynamics through Hydrogen Mass Repartitioning. *J. Chem. Theory Comput.* **2015**, *11*, 1864–1874. [[CrossRef](#)] [[PubMed](#)]
32. Andersen, H.C. Rattle: A “velocity” version of the shake algorithm for molecular dynamics calculations. *J. Comput. Phys.* **1983**, *52*, 24–34. [[CrossRef](#)]
33. Grest, G.S.; Kremer, K. Molecular dynamics simulation for polymers in the presence of a heat bath. *Phys. Rev. A* **1986**, *33*, 3628. [[CrossRef](#)]
34. Feller, S.E.; Zhang, Y.; Pastor, R.W.; Brooks, B.R. Constant pressure molecular dynamics simulation: The Langevin piston method. *J. Chem. Phys.* **1995**, *103*, 4613–4621. [[CrossRef](#)]
35. Jorgensen, W.L.; Chandrasekhar, J.; Madura, J.D.; Impey, R.W.; Klein, M.L. Comparison of simple potential functions for simulating liquid water. *J. Chem. Phys.* **1983**, *79*, 926–935. [[CrossRef](#)]
36. Humphrey, W.; Dalke, A.; Schulten, K. VMD—Visual Molecular Dynamics. *J. Mol. Graph.* **1996**, *14*, 33–38. [[CrossRef](#)]
37. De Paula, G.F.; Netto, G.I.; Mattoso, L.H.C. Physical and Chemical Characterization of Poly(hexamethylene biguanide) Hydrochloride. *Polymers* **2011**, *3*, 928–941. [[CrossRef](#)]
38. Williams, T.; Kelley, C. Gnuplot 5.0.6: An Interactive Plotting Program. 2017. Available online: <http://gnuplot.sourceforge.net/> (accessed on 5 August 2021).
39. McClellan, A.; Harnsberger, H. Cross-sectional areas of molecules adsorbed on solid surfaces. *J. Colloid Interface Sci.* **1967**, *23*, 577–599. [[CrossRef](#)]
40. Ikeda, T.; Tazuke, S.; Watanabe, M. Interaction of biologically active molecules with phospholipid membranes: I. Fluorescence depolarization studies on the effect of polymeric biocide bearing biguanide groups in the main chain. *Biochim. Biophys. Acta (BBA) Biomembr.* **1983**, *735*, 380–386. [[CrossRef](#)]
41. Ikeda, T.; Ledwith, A.; Bamford, C.; Hann, R. Interaction of a polymeric biguanide biocide with phospholipid membranes. *Biochim. Biophys. Acta (BBA) Biomembr.* **1984**, *769*, 57–66. [[CrossRef](#)]
42. Zaki, A.M.; Troisi, A.; Carbone, P. Unexpected Like-Charge Self-Assembly of a Biguanide-Based Antimicrobial Polyelectrolyte. *J. Phys. Chem. Lett.* **2016**, *7*, 3730–3735. [[CrossRef](#)]

43. Lin, J.; Alexander-Katz, A. Cell Membranes Open “Doors” for Cationic Nanoparticles/Biomolecules: Insights into Uptake Kinetics. *ACS Nano* **2013**, *7*, 10799–10808. [[CrossRef](#)]
44. Sowlati-Hashjin, S.; Carbone, P.; Karttunen, M. Insights into the Polyhexamethylene Biguanide (PHMB) Mechanism of Action on Bacterial Membrane and DNA: A Molecular Dynamics Study. *J. Phys. Chem. B* **2020**, *124*, 4487–4497. [[CrossRef](#)]
45. Fauquignon, M.; Ibarboure, E.; Carlotti, S.; Brûlet, A.; Schmutz, M.; Meins, J.F.L. Large and Giant Unilamellar Vesicle(s) Obtained by Self-Assembly of Poly(dimethylsiloxane)-b-poly(ethylene oxide) Diblock Copolymers, Membrane Properties and Preliminary Investigation of Their Ability to Form Hybrid Polymer/Lipid Vesicles. *Polymers* **2019**, *11*, 2013. [[CrossRef](#)] [[PubMed](#)]
46. Creppy, E.; Aboudoulatif, D.; Serge, M.; Eklü-Gadegbeku, C.; Cros, D. Study of Epigenetic Properties of Poly(HexaMethylene Biguanide) Hydrochloride (PHMB). *Int. J. Environ. Res. Public Health* **2014**, *11*, 8069–8092. [[CrossRef](#)] [[PubMed](#)]
47. Forrest, E.; Schulze, R.; Liu, C.; Dombrowski, D. Influence of surface contamination on the wettability of heat transfer surfaces. *Int. J. Heat Mass Transf.* **2015**, *91*, 311–317. [[CrossRef](#)]
48. Buser, D.; Brogini, N.; Wieland, M.; Schenk, R.; Denzer, A.; Cochran, D.; Hoffmann, B.; Lussi, A.; Steinemann, S. Enhanced Bone Apposition to a Chemically Modified SLA Titanium Surface. *J. Dent. Res.* **2004**, *83*, 529–533. [[CrossRef](#)] [[PubMed](#)]
49. MacDonald, D.; Deo, N.; Markovic, B.; Stranick, M.; Somasundaran, P. Adsorption and dissolution behavior of human plasma fibronectin on thermally and chemically modified titanium dioxide particles. *Biomaterials* **2002**, *23*, 1269–1279. [[CrossRef](#)]